



# CONTINUOUS SLIDING MODE APPROACH FOR A SELF-LIFT LUO CONVERTER VIA HIGH-ORDER SWITCHING MANIFOLD

ALIREZA GOUDARZIAN<sup>1</sup>

**Key words:** Power converter, Control design, Equivalent control technique.

A sliding mode duty ratio control is proposed for control of a positive output self-lift Luo converter. Conventional discontinuous sliding mode current method has been commonly used for switching dc/dc converters as it offers several benefits such as robust performance against operating point variations and easy implementation. However, this control strategy suffers from chattering phenomenon, due to its non-constant switching frequency. It makes the design of input and output filters more difficult and, it increases strongly electromagnetic interface (EMI) problem and inductor saturation possibility. To overcome the mentioned problems, this paper suggests a continuous sliding mode current control scheme based on a double-integral sliding surface. Contrary to the traditional controller, the proposed method can indirectly enforce the defined sliding variable to converge zero. The developed control technique provides not only the fixed switching frequency without chattering but also zero steady-state error and fast response. The modified sliding mode approach is applied to a positive output self-lift Luo converter in continuous conduction mode. The general control law of the proposed structure is derived using the equivalent control concept and the detailed stability of the closed loop system is investigated using sliding mode theory and small signal analysis. Moreover, practical results are provided to demonstrate the superior performance of the suggested sliding mode controller as compared with the existing methods.

## 1. INTRODUCTION

Boost dc/dc converters are widely recommended for many industrial sectors such as power supplies, wind energy, photovoltaic configurations and so on [1–8]. For this purpose, the boost [9], positive output elementary super lift Luo converter [10] and negative output Luo converter [11] can achieve a high voltage gain. Unfortunately, in practice, there is no any inductor (or capacitor) at the output (or input) node of these converters, which leads to a highly distorted output voltage and pulsating current. Also, both adding transformers and cascade connections can be applied to create new topologies with a high voltage gain [12]. However, additional problems are raised, such as large switching current surge, significant conduction and transformer core losses, high volume of these converters and control complexity. Recently, research has been focused on the transform-less voltage-lift power converters. This method is a good way to boost the output voltage in arithmetic progression. It is effectively used in design of transformerless single-switch converters. The voltage lift converters have been addressed in many literatures [13]. As a novel circuit solution, positive output self-lift Luo converter has the merits of non-pulsating output voltage with a very small ripple, step-up voltage gain and inherent protection against overload [14].

The research on the large-signal modeling and control strategy is essential to develop the industrial applications of dc/dc converters such as positive output self-lift Luo converter. In practice, diodes, circuit components and parametric resistances impact on the converter function and contribute to present voltage drops, resulting in a deviation between the practical output voltage and its theoretical value. Thus, a closed loop feedback control scheme is needed to obtain a regulated output voltage. The main objective of this paper is to perform the output voltage trajectory-tracking task of this converter.

There exists two major conventional techniques for modeling of high order complicated topologies; namely, signal flow graph and state-space modeling methods. The first method has been used for many power converters [12];

however, some components are ignored in the dynamical model, therefore, the closed loop system may be unstable against operating point variations of dc/dc converters. It creates the controller unsuitable for large signal models. Hence, in this paper, the state space averaging technique is applied to the positive output self-lift Luo converter.

From control viewpoint, many research studies have been focused on the output voltage control of dc/dc converters. The small-signal analysis is accomplished in [15] considering the parasitic elements. The design and analysis of a double loop proportional-integral (PI) controller is performed in [16] using the classical approaches. Conventional PI-type controllers are usually applied in industry, because of their simple design and ease of implementation. But these cannot predict the closed loop system response in a wide range of operation conditions.

Among nonlinear methods, the discrete real time modeling for digital control of pulse width modulation (PWM) converters has been suggested in [17]. Furthermore, the fuzzy-rule-based controllers have been presented for converters in [18], aiming to guarantee the output voltage convergence toward a particular value. However, these controllers have some drawbacks such as the unexpected complications in the stability analysis and the requirement of excessive amount of computation. It is broadly shown that variable structure methods such as sliding mode controller (SMC) are one of the best candidates to stabilize highly nonlinear time-varying switching converters [19].

It is a kind of nonlinear control strategies and can provide much better control performance particularly in some circumstance when the voltage of the input source or output resistance has a large range of change. In addition, hysteresis modulation-based sliding mode control (HMSMC) is a conventional approach applied in research for power converters. So far, various types of HMSMC such as simple and optimized methods are reported for power converters and other nonlinear systems in [20,21]. In this method, a discontinuous control law is utilized to force the designed sliding surface to approach zero from any initial conditions. The bad feature of HMSMC is that it has some switching

<sup>1</sup> Department of Electrical Engineering, Faculty of Technology and Engineering, Shahrekord University, Shahrekord, Iran  
Corresponding author email: alireza9071@gmail.com

properties, which occur at high frequency to remove deviations of sliding surface. However, from a practical viewpoint, real components cannot switch at very high frequencies. Therefore, a practical HMSMC operates at finite and non-constant switching frequency, resulting in chattering problem [22]. Accordingly, to eliminate the chattering phenomenon, different methods have been proposed in [23] to find a method to keep the switching frequency constant. There are three major techniques namely, the high order sliding mode method, the adaptive sliding mode control and indirect fixed frequency sliding mode controller. Although the first method cannot ensure that the SMC is continuous, the second controller can result in the robustness deterioration with respect to the system uncertainties, due to the mismatch between the adaptive observers and system plant.

To solve these problems, the third one is an effective method to deal with chattering without using discontinuous functions. On the other hand, constant frequency SMC is a continuous controller keeping all main features of traditional SMC when the disturbances exist in the system model. So far, the continuous sliding mode voltage controllers (CSMVC) with first order and second order sliding surface have been proposed for controlling the output voltage of the Boost converter in [24,25].

However, the non-minimum phase converters under the CSMVC should operate in a limited range of working conditions, otherwise, the closed loop system will be unstable. In the recent attempt for implementing other types of continuous SMCs with fixed frequency for non-minimum phase dc/dc converters, references [26,27] are adopted respectively, the simple continuous sliding mode current controller (CSMCC) and single integral-based continuous sliding mode current controller (SICSMCC), which can reduce the complexity, but not completely suppress the steady state error of the state variables of the converters. It is also understood that this steady state error varies as the operating point and switching frequency of the converter change. A perfect solution is adoption of high order sliding manifold.

Based on the mentioned discussions, the goal of this paper is to design an indirect CSMCC for a positive output self-lift Luo converter by using double-integral sliding surface and to improve the dynamical performance of the proposed system under large load and input voltage variations. The design procedure is done in three steps. First, using averaging technique derives the model of the positive output self-lift Luo converter. Then, an enhanced sliding manifold is defined by adding an integral term of the current and voltage error and double integral term of the voltage error to ensure the controller robustness and alleviate the steady state error of the output voltage of the converter. Finally, the controller parameters are selected by using the equivalent control technique.

The static and dynamic performances of the designed system are validated in various operating conditions and a comparison between the characteristics and properties of the proposed double-integral-based fixed frequency sliding mode current controller (DICSMCC) and simple continuous SMC is provided. The organization of this paper is as follows: In Section 2, circuit operation of the proposed converter is investigated, and key advantages of the converter are compared with other conventional converters. In Section 3, the proposed controller is designed based on the

converter model. In Section 4, the practical results are presented and finally, the conclusions are given in Section 5.

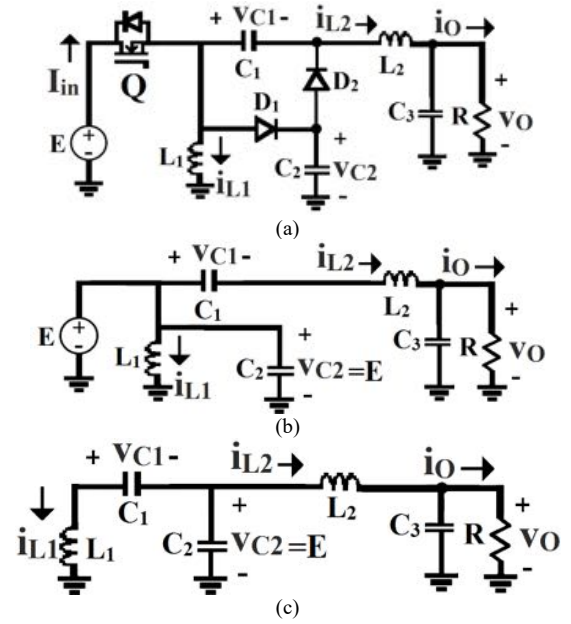


Fig. 1. – The power circuit of a self-lift positive output Luo converter; (a) topology; (b) the converter in the switch-ON mode; (c) the converter in the switch-OFF mode.

## 2. MODELING A POSITIVE OUTPUT SELF-LIFT LUO CONVERTER

The power circuit diagram of a positive output self-lift Luo converter is illustrated in Fig. 1a. It is comprised of a switch  $Q$ , two diodes  $D_1$  and  $D_2$ , three capacitors  $C_1$ ,  $C_2$  and  $C_3$ , and two inductors  $L_1$  and  $L_2$ .  $R$  is the symbol of output resistance. Also,  $v_{C1}$ ,  $v_{C2}$  and  $v_O$  are the voltage of capacitors  $C_1$ ,  $C_2$  and  $C_3$ , respectively.  $i_{L1}$  and  $i_{L2}$  are the current of the inductors  $L_1$  and  $L_2$ , respectively. Consider  $d$  as the duty cycle of the converter and  $T$  as the time period of the converter. In the time interval of  $0 < t < dT$ , switch is on,  $D_1$  conducts and  $D_2$  is in offstate. For this mode, the input inductor  $L_1$  and capacitor  $C_2$  are charged by input voltage  $E$ .

The capacitors  $C_1$ ,  $C_3$  and output inductor provide the energy to the output resistance. The first mode is shown in Fig. 1b. In the time interval of  $dT < t < T$ , the switch is off,  $D_2$  is in on-state and  $D_1$  off. In this condition,  $i_{L1}$  and  $v_{C2}$  supply the output energy. The second mode is shown in Fig. 1c. If value of the capacitor  $C_2$  is selected large enough, it is assumed that  $v_{C2}$  is constant and equal to  $E$  for all time periods. The converter works based on the PWM principles and is described in continuous conduction mode (CCM) by using the instantaneous model. The mathematical equation of the converter corresponding to Fig. 1b, can be obtained as follows:

$$\begin{aligned}
 L_1 \frac{di_{L1}}{dt} &= E, \\
 C_1 \frac{dv_{C1}}{dt} &= i_{L2}, \\
 L_2 \frac{di_{L2}}{dt} &= E - v_O - v_{C1}, \\
 C_3 \frac{dv_O}{dt} &= i_{L2} - \frac{v_O}{R}.
 \end{aligned}
 \tag{1} \text{ Switch-on mode}$$

The mathematical equation of the converter that corresponds to Fig. 1c, can be expressed as follows:

$$\begin{aligned}
L_1 \frac{di_{L1}}{dt} &= E + v_{C1}, \\
C_1 \frac{dv_{C1}}{dt} &= -i_{L1}, \\
L_2 \frac{di_{L2}}{dt} &= E - v_O, \\
C_3 \frac{dv_O}{dt} &= i_{L2} - \frac{v_O}{R}.
\end{aligned}
\quad \text{Switch-off mode} \quad (2)$$

Combining the above equations, the state-space equation of the converter is given as follows:

$$\begin{aligned}
L_1 \frac{di_{L1}}{dt} &= E + (1-u)v_{C1}, \\
C_1 \frac{dv_{C1}}{dt} &= ui_{L2} - (1-u)i_{L1}, \\
L_2 \frac{di_{L2}}{dt} &= E - v_O - uv_{C1}, \\
C_3 \frac{dv_O}{dt} &= i_{L2} - \frac{v_O}{R},
\end{aligned}
\quad (3)$$

where  $u$  is "1" for the switch-on mode and "0" for the switch-off mode. By considering the time-derivative of all the variables to be equal to zero, due to the quantities are almost constant, the equilibrium point of the positive output self-lift Luo is given in (4).

$$I_{L1} = \frac{d}{1-d} \frac{V_O}{R}, V_{C1} = -V_O, I_{L2} = \frac{V_O}{R}. \quad (4)$$

Also,  $V_O$ ,  $I_{L1}$ ,  $V_{C1}$ ,  $V_{C2}$ ,  $I_{L2}$  are the average value of  $v_O$ ,  $i_{L1}$ ,  $v_{C1}$ ,  $v_{C2}$ ,  $i_{L2}$  in steady state region, respectively.

### 3. FIXED FREQUENCY SLIDING MODE CURRENT CONTROLLER (FFSMCC) BASED ON HIGH-ORDER SLIDING SURFACE

The proposed CSMCC for the positive output self-lift Luo converter is defined as follows:

$$\begin{aligned}
S &= \alpha_1(i_{L1} - I_d) + \alpha_2(\beta v_O - V_d) + \alpha_3 \int_0^t (i_{L1} - I_d) dt \\
&+ \alpha_4 \int_0^t (\beta v_O - V_d) dt + \alpha_5 \int_0^t \left[ \int_0^t (\beta v_O - V_d) dt \right] dt,
\end{aligned}
\quad (5)$$

where  $\alpha_1$ ,  $\alpha_2$ ,  $\alpha_3$  and  $\alpha_4$  are the controller parameters,  $\beta$  is scaling factor,  $I_d$  and  $V_d$  are the reference signal of the inductor current and output voltage. At the beginning of the controller design, it is remarked that the controlled state variables are the inductor current error ( $i_{L1}$ ) and output voltage error ( $v_O$ ) of the converter. The logic function  $u = 0.5(1 + \text{sign}(S))$  shows the two-states position of the switch for reaching condition of phase trajectories. By using the converter's behavioral model under supposition of CCM operation, the time derivative of (5) can be given as:

$$\begin{aligned}
\frac{dS}{dt} &= \frac{\alpha_1}{L_1} E + \frac{\alpha_1}{L_1} (1-u)v_{C1} + \frac{\alpha_2 \beta}{C_3} i_{CO} + \alpha_3 (i_{L1} - I_d) + \\
&\alpha_4 (\beta v_O - V_d) + \alpha_5 \int_0^t (\beta v_O - V_d) dt,
\end{aligned}
\quad (6)$$

where  $i_{CO}$  denotes the instantaneous current of the output capacitor. The equivalent control signal of the proposed

system is determined by solving  $\frac{dS}{dt} = 0$ , which gives eq. (7). Also, the parameters of this equation are shown in (8).  $u_{eq}$  is bounded and continuous and takes values in the interval of  $[0,1]$ . It is noticed that the gain  $\alpha_1$  is intentionally used to keep the denominator of the obtained signal at a limited amount level in practice. The developed CSMCC, which works at a constant frequency, is constructed via a pulse width modulation (PWM) scheme by using a set of derived control laws.

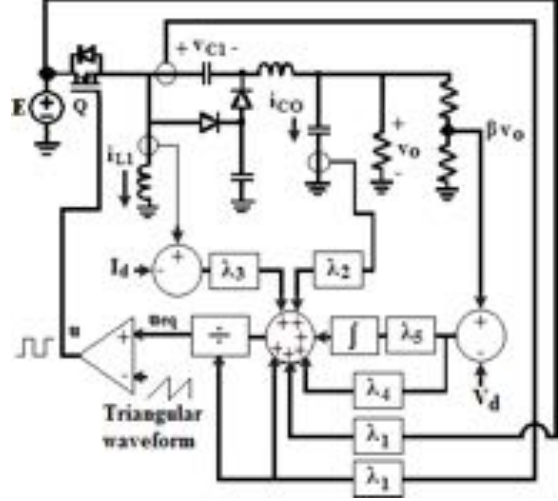


Fig. 2. – The proposed DICSMC for positive output self-lift Luo converter.

Figure 2 indicates an overview of the proposed CSMCC for the positive output self-lift Luo converter. It should be noticed that two current sensors are used for the controller implementation. But the inductor current should be essentially measured to provide a robust response for right-half-plane-zero (RHPZ) system.

$$\begin{aligned}
&\lambda_1 v_{C1} + \lambda_1 E + \lambda_2 i_{CO} + \lambda_3 (i_{L1} - I_d) + \\
&\lambda_4 (\beta v_O - V_d) + \lambda_5 \int_0^t (\beta v_O - V_d) dt \\
u_{eq} &= \frac{\lambda_1 v_{C1}}{\lambda_1 v_{C1}}, \quad (7)
\end{aligned}$$

$$\lambda_1 = \alpha_1, \lambda_2 = \frac{L_1 \alpha_2 \beta}{C_3}, \lambda_3 = L_1 \alpha_3, \lambda_4 = L_1 \alpha_4, \lambda_5 = L_1 \alpha_5. \quad (8)$$

#### 3.1 PARAMETER SELECTION

The invariance condition guarantees the system stability in any equilibrium point. By checking the condition, the suitable range of the controller gains is achieved. The sliding manifold designed in this research for the DICSMCC comprises both the current and voltage as state-space variables. The selection of the controller parameter to attain the invariance condition isn't inherently performed as in voltage-controlled systems by designing the controller-converter system for some predicted dynamical properties. Hence, this paper uses the equivalent control method and to obtain the controller coefficients. The stability condition should be investigated on its equilibrium point by determining the dynamical equation of the converter. Based on the equivalent control principles [21,22], the switch status ( $u$ ) of the converter in (3) should be substituted by  $u_{eq}$  to obtain the ideal dynamical equation of the converter under the proposed controller as (9).

$$\begin{aligned}
L_1 \frac{di_{L1}}{dt} &= E + (1 - u_{eq})v_{C1}, \\
C_1 \frac{dv_{C1}}{dt} &= u_{eq}i_{L2} - (1 - u_{eq})i_{L1}, \\
L_2 \frac{di_{L2}}{dt} &= E - v_O - u_{eq}v_{C1}, \\
C_3 \frac{dv_O}{dt} &= i_{L2} - \frac{v_O}{R}.
\end{aligned} \tag{9}$$

Equation (9) is used to show the closed-loop stability. The By substituting (7) into (9), equation (10) can be given. It is assumed that a stable equilibrium point exists on the sliding manifold when the state errors are finally settled. This point of equilibrium can be obtained by (4). The ideal dynamics of the controlled system (10) can be expanded into DC and AC terms expressed in equation (11).

$$\begin{aligned}
L_1 \frac{di_{L1}}{dt} &= \\
& - \frac{\lambda_3}{\lambda_1} (i_{L1} - I_d) - \frac{\lambda_2}{\lambda_1} i_{L2} + \frac{\lambda_2}{R\lambda_1} v_O -
\end{aligned} \tag{10-a}$$

$$- \frac{\lambda_4}{\lambda_1} (\beta v_O - V_d) - \frac{\lambda_5}{\lambda_1} \int_0^t (\beta v_O - V_d) dt,$$

$$\begin{aligned}
C_1 \frac{dv_{C1}}{dt} &= \\
& \left[ \lambda_1 E + \lambda_2 (i_{L2} - v_O/R) + \lambda_3 (i_{L1} - I_d) + \right. \\
& \left. + \lambda_4 (\beta v_O - V_d) + \lambda_5 \int_0^t (\beta v_O - V_d) dt \right] \times \\
& \times \frac{(i_{L2} + i_{L1})}{\lambda_1 v_{C1}} + i_{L2},
\end{aligned} \tag{10-b}$$

$$C_3 \frac{dv_O}{dt} = i_{L2} - \frac{v_O}{R}, \tag{10-d}$$

$$\begin{aligned}
L_1 \frac{d(I_{L1} + \tilde{i}_{L1})}{dt} &= \\
& - \frac{\lambda_3}{\lambda_1} (I_{L1} + \tilde{i}_{L1} - I_d - \tilde{i}_d) - \frac{\lambda_2}{\lambda_1} (I_{L2} + \tilde{i}_{L2}) + \\
& + \frac{\lambda_2}{R\lambda_1} (V_O + \tilde{v}_O) - \frac{\lambda_4}{\lambda_1} (\beta V_O + \beta \tilde{v}_O - V_d - \tilde{v}_d) -
\end{aligned} \tag{11-a}$$

$$- \frac{\lambda_5}{\lambda_1} \int_0^t (\beta V_O + \beta \tilde{v}_O - V_d - \tilde{v}_d) dt$$

$$\begin{aligned}
C_1 \frac{d(V_{C1} + \tilde{v}_{C1})}{dt} &= \\
& \left[ \lambda_1 E + \lambda_2 (I_{L2} + \tilde{i}_{L2} - V_O/R - \tilde{v}_O/R) + \right. \\
& \left. + \lambda_3 (I_{L1} + \tilde{i}_{L1} - I_d - \tilde{i}_d) + \right. \\
& \left. + \lambda_4 (\beta V_O + \beta \tilde{v}_O - V_d - \tilde{v}_d) + \right. \\
& \left. + \lambda_5 \int_0^t (\beta V_O + \beta \tilde{v}_O - V_d - \tilde{v}_d) dt \right] \times
\end{aligned} \tag{11-b}$$

$$\times \frac{I_{L2} + \tilde{i}_{L2} + I_{L1} + \tilde{i}_{L1}}{\lambda_1 (V_{C1} + \tilde{v}_{C1})} + I_{L2} + \tilde{i}_{L2},$$

$$\begin{aligned}
L_2 \frac{d(I_{L2} + \tilde{i}_{L2})}{dt} &= \\
& = E - V_O - \tilde{v}_O - \tilde{v}_{C1} - V_{C1} - \\
& - E - \frac{\lambda_2}{\lambda_1} (I_{L2} + \tilde{i}_{L2}) + \frac{\lambda_2}{R\lambda_1} (V_O + \tilde{v}_O) -
\end{aligned} \tag{11-c1}$$

$$\begin{aligned}
& - \frac{\lambda_3}{\lambda_1} (I_{L1} + \tilde{i}_{L1} - I_d - \tilde{i}_d) - \\
& - \frac{\lambda_4}{\lambda_1} (\beta V_O + \beta \tilde{v}_O - V_d - \tilde{v}_d) -
\end{aligned} \tag{11-c2}$$

$$\begin{aligned}
& - \frac{\lambda_5}{\lambda_1} \int_0^t (\beta V_O + \beta \tilde{v}_O - V_d - \tilde{v}_d) dt, \\
C_3 \frac{d(V_O + \tilde{v}_O)}{dt} &= I_{L2} + \tilde{i}_{L2} - \frac{V_O + \tilde{v}_O}{R},
\end{aligned} \tag{11-d}$$

$$\begin{aligned}
L_1 \frac{d\tilde{i}_{L1}}{dt} &= \\
& - \frac{\lambda_3}{\lambda_1} \tilde{i}_{L1} - \frac{\lambda_2}{\lambda_1} \tilde{i}_{L2} + \frac{\lambda_2}{R\lambda_1} \tilde{v}_O -
\end{aligned} \tag{12-a}$$

$$\begin{aligned}
& - \frac{\lambda_4}{\lambda_1} \beta \tilde{v}_O - \frac{\lambda_5}{\lambda_1} \int_0^t (\beta \tilde{v}_O - \tilde{v}_d) dt + \\
& + \frac{\lambda_3}{\lambda_1} \tilde{i}_d + \frac{\lambda_4}{\lambda_1} \tilde{v}_d,
\end{aligned}$$

$$\begin{aligned}
C_1 \frac{d\tilde{v}_{C1}}{dt} &= \\
& - \left( \frac{E}{V_O} + \frac{\lambda_3 V_O}{\lambda_1 R E} \right) \tilde{i}_{L1} + \left( 1 - \frac{E}{V_O} - \frac{\lambda_2 V_O}{\lambda_1 R E} \right) \tilde{i}_{L2} +
\end{aligned} \tag{12-}$$

$$\begin{aligned}
& + \frac{\lambda_2 V_O}{\lambda_1 R^2 E} \tilde{v}_O - \frac{\lambda_4 V_O}{\lambda_1 R E} \beta \tilde{v}_O - \frac{\lambda_5 V_O}{\lambda_1 R E} \int_0^t (\beta \tilde{v}_O - \tilde{v}_d) dt + \\
& + \frac{\lambda_3 V_O}{\lambda_1 R E} \tilde{i}_d + \frac{\lambda_4 V_O}{\lambda_1 R E} \tilde{v}_d,
\end{aligned}$$

$$\begin{aligned}
L_2 \frac{d\tilde{i}_{L2}}{dt} &= \\
& - \frac{\lambda_3}{\lambda_1} \tilde{i}_{L1} - \frac{\lambda_2}{\lambda_1} \tilde{i}_{L2} - \tilde{v}_O - \tilde{v}_{C1} + \\
& + \frac{\lambda_2}{R\lambda_1} \tilde{v}_O - \frac{\lambda_4}{\lambda_1} \beta \tilde{v}_O - \frac{\lambda_5}{\lambda_1} \int_0^t (\beta \tilde{v}_O - \tilde{v}_d) dt + \\
& + \frac{\lambda_3}{\lambda_1} \tilde{i}_d + \frac{\lambda_4}{\lambda_1} \tilde{v}_d,
\end{aligned} \tag{12-c}$$

$$C_3 \frac{d\tilde{v}_O}{dt} = \tilde{i}_{L2} - \frac{\tilde{v}_O}{R}, \tag{12-d}$$

$$\frac{d}{dt} \int_0^t (\beta \tilde{v}_O - \tilde{v}_d) dt = \beta \tilde{v}_O - \tilde{v}_d. \tag{12-e}$$

The dc terms are equal to their desirable values. Also, these are constant and much larger than ac expressions. Thus, the following relations are valid:  $\beta V_O - V_d = 0$ ,  $I_{L1} - I_d = 0$ ,  $\frac{dI_{L1}}{dt} = 0$ ,  $\frac{dV_{C1}}{dt} = 0$ ,  $\frac{dI_{L2}}{dt} = 0$ ,  $\frac{dV_O}{dt} = 0$ ,  $I_{L1} \gg \tilde{i}_{L1}$ ,  $V_{C1} \gg \tilde{v}_{C1}$ ,  $I_{L2} \gg \tilde{i}_{L2}$ ,  $V_O \gg \tilde{v}_O$ ,  $V_d \gg \tilde{v}_d$ ,  $I_d \gg \tilde{i}_d$ . Using these steady state conditions and after some manipulations, eq. (11) can be simplified as eq. (12). Let  $\tilde{V}_O(s)$  and  $\tilde{V}_d(s)$  be the Laplace transforms of  $\tilde{v}_O$  and  $\tilde{v}_d$ , respectively where  $s$  is the complex frequency. After using Laplace transform, the transfer function of eq. (12) can be

obtained as follows:

$$\frac{\tilde{V}_O(s)}{\tilde{V}_d(s)} = \frac{b_3s^3 + b_2s^2 + b_1s + b_0}{a_5s^5 + a_4s^4 + a_3s^3 + a_2s^2 + a_1s + a_0}, \quad (13)$$

where  $b_3 = \lambda_4 C_1 L_1 RE V_O$ ,  $b_2 = \lambda_5 C_1 L_1 RE V_O - \lambda_4 L_1 V_O^2$ ,  
 $b_1 = \lambda_4 RE^2 - \lambda_5 L_1 V_O^2$ ,  $b_0 = \lambda_5 RE^2$ ,  $a_5 = \lambda_1 C_1 C_3 L_1 L_2 RE V_O$ ,  
 $a_4 = \lambda_1 C_1 EL_1 L_2 V_O + \lambda_2 C_1 C_3 EL_1 RV_O + \lambda_3 C_1 C_3 EL_2 RV_O$ ,  
 $a_3 = -\lambda_2 C_3 L_1^2 + \lambda_1 C_3 L_1 RE V_O$   
 $+ \lambda_1 C_1 L_1 RE V_O + \lambda_3 C_1 L_2 EV_O - \lambda_1 C_3 L_1 RE^2 + \beta \lambda_4 C_1 L_1 RE V_O$ ,  
 $a_2 = -\lambda_1 L_1 E^2 + \lambda_1 L_1 EV_O + \lambda_2 C_3 RE^2 - \lambda_3 C_3 RE^2 - \beta \lambda_4 L_1 V_O$   
 $- \lambda_3 E^2 + \beta \lambda_4 RE^2 - \beta \lambda_5 L_1 V_O^2$ ,  $a_0 = \beta \lambda_5 RE^2$ .

The transfer function (13) has been obtained starting from the mathematical model (12). Next, by using the Routh-Hurwitz criterion and to have a stable system, the condition (14) should be fulfilled.

$$a_0 > 0, \quad (14-a)$$

$$a_4 > 0, \quad (14-b)$$

$$a_5 > 0, \quad (14-c)$$

$$\frac{a_3 a_4 - a_2 a_5}{a_4} > 0, \quad (14-d)$$

$$\frac{a_2(a_3 a_4 - a_2 a_5) - a_4^2(a_1 a_2 - a_0 a_3)}{a_2(a_3 a_4 - a_2 a_5)} > 0, \quad (14-e)$$

$$\frac{a_1 a_2 - a_0 a_3}{a_2} - \frac{-a_0 a_2(a_3 a_4 - a_2 a_5)^2}{a_4 a_2^2(a_3 a_4 - a_2 a_5) - a_4^3(a_1 a_2 - a_0 a_3)} > 0. \quad (14-f)$$

Solving eqs. (14a-d), it yields:

$$\lambda_1, \lambda_2, \lambda_3, \lambda_5 > 0. \quad (15)$$

It is hard to provide an analytical solution for (14a-f). Hence, the numerical method should be applied to find the solutions to guarantee (14a-f). For simplicity, it is assumed that the scaling factors  $\lambda_1$  and  $\beta$  are 0.1. The parameters of the converter are listed in Table 1. The range of the controller coefficient for satisfaction of inequities (14a-f) is shown in Fig. 3. Hence, the synthesis of the controller gains should provide a solution within the obtained region to ensure stability. There are infinite numbers of solutions for  $\lambda_2$ ,  $\lambda_3$ ,  $\lambda_4$  and  $\lambda_5$ . The parameter design can be explored by investigating the frequency domain performance of the proposed system. The appropriate performance is given from the simulations and the practical results with the phase margin 68.5 at the gain crossover frequency of 1651 Hz for operating point of  $V_O = 36$  V,  $E = 12$  V,  $R = 36$   $\Omega$ . Hence, the constants of  $\lambda_2 = 0.5$ ,  $\lambda_3 = 1$ ,  $\lambda_4 = 1$  and  $\lambda_5 = 500$  are chosen heuristically to show the desired results.

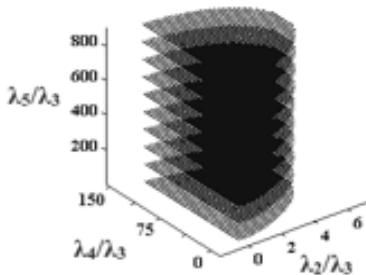


Fig. 3 – The range of the controller parameters corresponding to Routh-Hurwitz criterion.

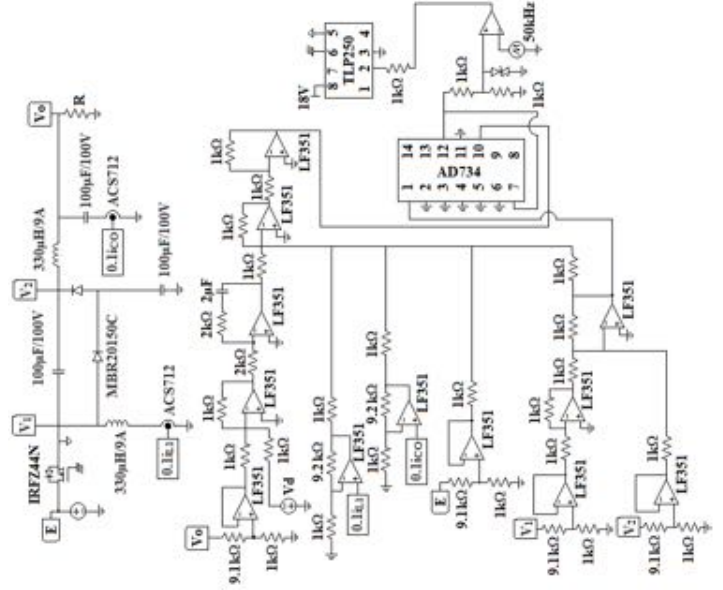


Fig. 4 – Configuration of the positive output self-lift Luo converter circuit with the designed DICSMMC.

## 4. RESULTS AND DISCUSSIONS

The proposed controller performance for the converter is verified in various conditions via practical results. Furthermore, an experimental set-up of the designed DICSMMC has been constructed in analogue platforms. In practice, analogue implementation is preferred to digital control, due to high sampling frequency. Table 1 shows the specification of a low power positive output self-lift Luo converter used in this paper. The improved DICSMMC is designed to provide an under damped behavior with fast response.

Table 1

Nominal parameters of the proposed system.

Parameter	Symbol	Value
Minimum input voltage	$E_{\min}$	9 V
Maximum input voltage	$E_{\max}$	18 V
Nominal output voltage	$V_O$	36 V
Minimum output current	$I_{O\min}$	0.375 A
Maximum output current	$I_{O\max}$	1 A
Minimum output power	$P_{O\min}$	13.5 W
Maximum output power	$P_{O\max}$	36 W
Selected inductors	$L_1, L_2$	330 $\mu$ H, 600 $\mu$ H
Selected capacitors	$C_1, C_2, C_3$	100 $\mu$ F
Output resistance	$R$	36, 48, 96 $\Omega$
Nominal switching frequency	$f_s$	50 kHz

Figure 4 shows the full schematic diagram of the converter with the DICSMMC. IRFZ44N and MBR20150C are chosen for power switch and diodes [28,29]. The input and output inductors with ferrite core and value of 330  $\mu$ H/10 A and 600  $\mu$ H/5A and three electrolytic capacitors with the value of 100  $\mu$ F/100V are used in the prototype circuit. The input inductance and output capacitor currents are measured using the ACS712-20A sensors [30] and, the voltage measurement is done applying the resistive dividers.

In this work, the high slew rate OP-AMP LF351 is used for the signal amplification [31]. Furthermore, an optocoupler device TLP250 is utilized to isolate the control circuit from power stage [32]. In addition, AD734 IC is used for division operation [33], and the switching frequency is set at 50 kHz. To

show the controller robustness, the desired current signal  $I_d$  is disabled. Different experiments are performed for evaluation of the control scheme performance with respect to output load control and line control. It is assumed that the converter operates under the condition of 9 V input voltage and  $V_d \cong 3.6$  V. The transient waveforms of the output voltage and inductor current are observed to validate the stability performance. The system response is shown in Figs. 5a-c for different output resistances, i.e. 36, 48 and 96  $\Omega$ , respectively. It can be easily seen that for these cases, the output voltage and current are reached from zero to steady state region with settling time of less than about 50 ms for all conditions. Moreover, under the condition of 36 V output voltage and 36  $\Omega$  load, the dynamic behavior in the start-up region is observed to show stability performance.

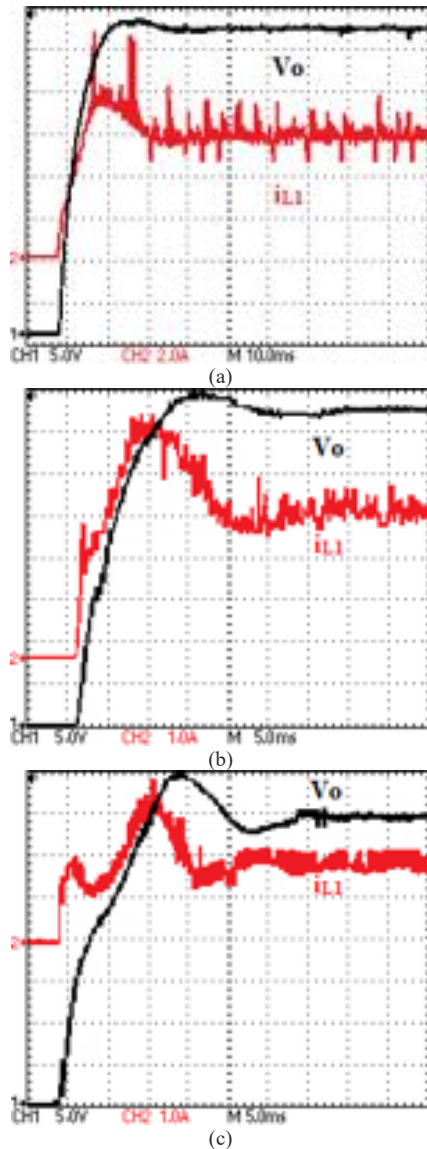


Fig. 5 – Output voltage and inductor current waveforms of a positive output self-lift Luo converter with a 9V input voltage, output voltage of about 36 V; (a)  $R = 36 \Omega$ ; (b)  $R = 48 \Omega$ ; (c)  $R = 96 \Omega$

Here, the control performance of the proposed controller for the Luo converter is evaluated and compared with the simple CSMCC against load and input voltage variations. In the case of both controllers, the converter operates at 36 V output voltage, 12 V input voltage and 48  $\Omega$  load resistance in steady state region. The output resistance is suddenly changed from

48 to 96  $\Omega$ . The experimental results for this condition are shown in Fig. 6.

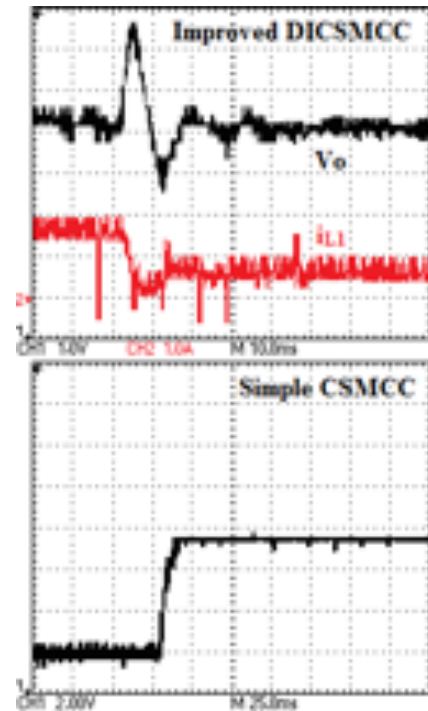


Fig. 6 – The dynamic response of the improved and simple controller against load changes for  $E = 12$  V and the load steps-up from 48 to 96  $\Omega$ .

It can be observed that the voltage overshoot is 2 V and settling time is about 20 ms. However, in the case of the simple CSMCC the voltage cannot return to initial condition after the change. Also, assuming the output load of the converter steps-down from 48 to 36  $\Omega$ . The practical behavior of the converter voltage for this condition is illustrated in Fig. 7 for the improved DICS MCC and simple CSMCC.

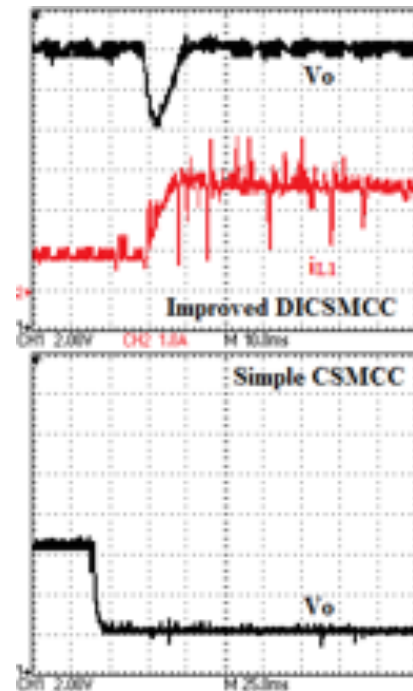


Fig. 7 – The dynamic response of the improved and simple controller against load changes for  $E = 12$  V and the load steps-down from 48 to 36  $\Omega$ .

From these figures, it is inferred that the output voltage with the simple CSMCC suffers from a large steady state error after

the variations.

Analogously, the dynamic performance of the converter with the improved and simple controllers against the input source voltage variation is verified. The nominal value of the output resistance  $R$ , input voltage and output voltage are set at  $48 \Omega$ ,  $18 \text{ V}$  and  $36 \text{ V}$ . The input voltage is dropped to below  $10 \text{ V}$ . The experimental results are depicted in Fig. 8. In the case of improved DICSMCC, the output voltage goes back to  $36 \text{ V}$  after  $30 \text{ ms}$ . However, the output voltage of the Luo converter with the simple CSMC has a larger error of about  $6 \text{ V}$  after this change. Therefore, it can be understood that the proposed DICSMCC can well regulate the output voltage with a good transient performance for the large change of the input voltage (for example  $50\%$  drop).

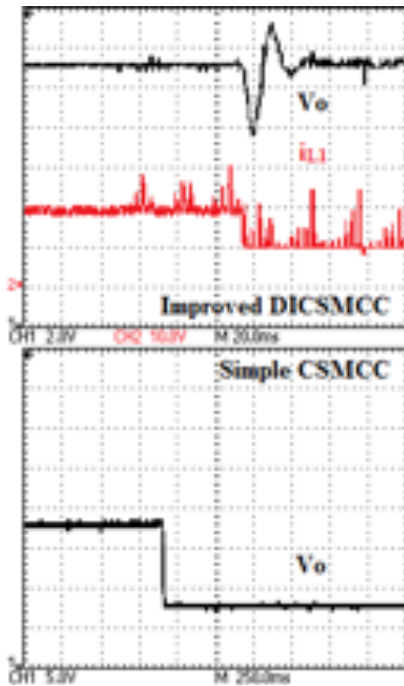


Fig. 8 – The dynamic response of the output voltage against input voltage changes from  $18$  to  $9 \text{ V}$  for  $R = 48 \Omega$  for the improved controller and simple controller.

Furthermore, the excellent consistency of the dynamic response evidently confirms the superior characteristics of the developed controller for large parametric fluctuations.

## 5. CONCLUSION

In this paper, a continuous sliding mode controller with fixed switching frequency has been designed for output voltage control of a positive output self-lift Luo converter in CCM operating conditions based on the high order sliding surface to eliminate the chattering problem of hysteresis modulation sliding mode controllers. The parameters of the proposed control method have been obtained based on making the converter system stable and robust against parametric uncertainties, load variations and with respect to disturbances of the input voltage. A simple PI compensator in cascade with a first order sliding mode controller or two cascaded conventional PI compensators can also be used for output voltage control of the Luo converter. However, these control strategies are not strong with respect to converter uncertainties, load disturbances and parameter variations as mentioned above. Furthermore, two cascaded first order sliding mode controller has been used for comparison in this paper. Using analogue components, the effectiveness and

accuracy of the proposed approach has been investigated by practical results. It will be helpful to enrich the understanding and promote the practical aspects corresponding to high-order complicated dc/dc converters.

Received on August 3, 2020

## REFERENCES

1. B. Anton, A. Florescu, L. A. Perisoara, A. Vasile, R. Constanescu, S. G. Rosu, *Methods of maximizing power efficiency for hybrid vehicles*, Rev. Roum. Sci. Techn. – Électrotechn. Et Énerg., **64**, 1, pp. 57–62 (2019).
2. A. Goudarzian, *Design, analysis and control of a quasi-resonant Luo converter with a high voltage gain*, Rev. Roum. Sci. Techn. – Électrotechn. Et Énerg., **64**, 3, pp. 267–274 (2019).
3. A. Goudarzian, A. Khosravi, H. A. Raeisi, *Modeling and implementation of a new boost converter with elimination of right-half-plane zero*, Int. Trans. Electr. Energy Syst., **30**, 9, e12476 (2020).
4. A. Goudarzian, A. Khosravi, H. A. Raeisi, *Analysis of a step-up dc/dc converter with capability of right-half plane zero cancellation*, Renew. Energy., **157**, pp. 1156–1170 (2020).
5. A. Goudarzian, *A new technique for right half plane zero elimination from dynamics of a boost converter using magnetic coupling concept*, Circuit World., (2021), doi: 10.1108/CW-01-2021-0013.
6. A. Goudarzian, A. Khosravi, H. A. Raeisi, *Modeling, design and control of a modified flyback converter with ability of right-half-plane zero alleviation in continuous conduction mode*, Eng. Sci. Technol., (2021), doi: 10.1016/j.jestech.2021.05.011.
7. A. Benaissa, B. Rabhi, M. F. Benkhoris, L. Zellouma, *Linear quadratic controller for two-interleaved boost converter associated with PEMFC emulator*, Rev. Roum. Sci. Techn. – Électrotechn. Et Énerg., **66**, 2, pp. 125–130 (2021).
8. T. Huynh Van, T. Le Van, T. M. Nguyen Thi, M. Q. Duong, G. N. Sava, *Improving the output of DC-DC converter by phase shift full bridge applied to renewable energy*, Rev. Roum. Sci. Techn. – Électrotechn. Et Énerg., **66**, 3, pp. 175–180 (2021).
9. A. Attou, A. Massoum, M. Chadli, *Comparison study of two tracking methods for photovoltaic systems*, Rev. Roum. Sci. Techn. – Électrotechn. Et Énerg., **60**, 2, pp. 205–214 (2015).
10. H. Nasiri, A. Goudarzian, R. Pourbagher, S. Y. Derakhshandeh, *PI and PWM sliding mode control of POESLL converter*, IEEE Trans. Aerosp. Electron. Syst., **53**, 5, pp. 2167–2177, (2017).
11. K. Kumar, S. Jeevananthan, *Design and implementation of reduced-order sliding mode controller plus proportional double integral controller for negative output elementary super-lift Luo-converter*, IET Power Electron., **6**, 5, pp. 974–989 (2013).
12. B. Axelrod, Y. Berkovich, A. Ioinovici, *Switched-capacitor/switched-inductor structures for getting transformerless hybrid dc/dc PWM converters*, IEEE Trans. Circuits Syst. I, Regul. Pap., **55**, 2, 687–696 (2008).
13. A. Goudarzian, A. Khosravi, *Application of dc/dc Cuk converter as a soft starter for battery chargers based on double-loop control strategy*, Int. J. Circuit Theory Appl., **47**, 5, 753–781 (2019).
14. F. L. Luo, H. Ye, *Advanced dc/dc converters*, CRC Press and Taylor & Francis Group, London, New York, 2006.
15. J. Liu, J. Hu, L. Xu, *Dynamic modeling and analysis of Z source converter-derivation of AC small signal model and design-oriented analysis*, IEEE Trans. Power Electron., **22**, 5, pp. 1786–1796 (2007).
16. D. Maksimovic, R. Zane, *Small-signal discrete-time modeling of digitally controlled PWM converters*, IEEE Trans. Power Electron., **22**, 6, pp. 2552–2556 (2007).
17. M. Shirazi, R. Zane, D. Maksimovic, *An auto tuning digital controller for dc/dc power converters based on online frequency response measurement*, IEEE Trans. Power Electron., **24**, 11, pp. 2578–2588 (2009).
18. S. M. Rakhtala, E. S. Roudbari, *Fuzzy PID control of a stand-alone system based on PEM fuel cell*, Int. J. Electr. Power Energy Syst., **78**, pp. 576–590 (2016).
19. A. Mouradi, G. Keltoum, *Power system stabilizer based on terminal sliding mode control*, Rev. Roum. Sci. Techn. – Électrotechn. Et Énerg., **62**, 1, pp. 98–102 (2017).
20. W. Qi, S. Li, S. Tan, S. Hui, *Parabolic-modulated sliding mode voltage control of buck converter*, IEEE Trans. Ind. Electron., **65**, 1, pp. 844–954 (2018).
21. A. Goudarzian, A. Khosravi, N. R. Abjadi, *Sliding mode current control*

- of a NOCULL converter based on hysteresis modulation method in a wide range of operating conditions, *ISA Trans. Elsevier J.*, **85**, pp. 214–225 (2019).
22. A. Goudarzian, A. Khosravi, H. A. Raeisi, *Optimized sliding mode current controller for power converters with non-minimum phase nature*. *J. Frankl. Inst. Elsevier. J.*, **356**, *15*, pp. 8569–8594 (2019).
  23. V. Acary, B. Brogliato, Y. V. Orlov, *Chattering-free digital sliding mode control with state observer and disturbance rejection*, *IEEE Trans. Autom. Control.*, **57**, *5*, pp. 1087–1101 (2012).
  24. T. Gonzalez, J. A. Moreno, L. Fridman, *Variable gain super twisting sliding mode control*, *IEEE Trans. Autom. Control.*, **57**, *8*, 2100–2105 (2012).
  25. S. H. Chincholkar, C. Y. Chan, *Design of fixed-frequency pulse-width modulation-based sliding-mode controllers for the quadratic boost converter*, *IEEE Trans. Circuits Syst. II, Exp. Briefs.*, **64**, *1*, pp. 51–55 (2017).
  26. E. Vidal-Idiarte, A. Marcos-Pastor, G. Garcia, A. Cid-Pastor, L. Martinez-Salamero, *Discrete-time sliding-mode-based digital pulse width modulation control of a boost converter*, *IET Power Electron.*, **8**, *5*, pp. 708–714 (2015).
  27. M. Gao, D. Wang, Y. Li, T. Yuan, *Fixed frequency pulse-width modulation based integrated sliding mode controller for phase-shifted full-bridge converters*, *IEEE Access.*, **6**, pp. 2181–2192 (2017).
  28. \*\*\*International IOR Rectifier, *IRFZ44N*, [www.datasheet.octopart.com/IRFZ44N-Inchange-Semiconductor-datasheet-15981338.pdf](http://www.datasheet.octopart.com/IRFZ44N-Inchange-Semiconductor-datasheet-15981338.pdf).
  29. \*\*\*Unisonic Technologies, *MBR20150C*, [www.datasheet39.com/PDF/952071/MBR20150C-datasheet.html](http://www.datasheet39.com/PDF/952071/MBR20150C-datasheet.html).
  30. \*\*\*Allegro MicroSystems, *ACS712*, [www.sparkfun.com/datasheets/BreakoutBoards/0712.pdf](http://www.sparkfun.com/datasheets/BreakoutBoards/0712.pdf).
  31. \*\*\*Fairchild Semiconductor, *LF351*, [www.mouser.com/datasheet/2/308/LF351-1192635.pdf](http://www.mouser.com/datasheet/2/308/LF351-1192635.pdf).
  32. \*\*\*Toshiba, *TLP250*, [www.datasheetspdf.com/pdf-file/318802/ToshibaSemiconductor/TLP250/1](http://www.datasheetspdf.com/pdf-file/318802/ToshibaSemiconductor/TLP250/1).
  33. \*\*\*Analog Devices, *10 MHz, Four-Quadrant Multiplier/Divider AD734*, [www.analog.com/media/en/technical-documentation/data-sheets/AD734.pdf](http://www.analog.com/media/en/technical-documentation/data-sheets/AD734.pdf).